Supporting Information:

Physicochemical Concepts of the Lithium Metal Anode in Solid-State Batteries

Thorben Krauskopf[1,], Felix H. Richter[1,2], Wolfgang G. Zeier[3] and Jürgen Janek[1,2,*]*

[1]Institute of Physical Chemistry, Justus-Liebig-University Giessen, Heinrich-Buff-Ring 17, D-35392 Giessen, Germany.

[2]Center for Materials Research (LaMa), Justus-Liebig-University Giessen, Heinrich-Buff-Ring 16, D-35392 Giessen, Germany.

[3]Institute of Inorganic and Analytical Chemistry, University of Münster, Corrensstrasse 30, 48149 Münster, Germany.

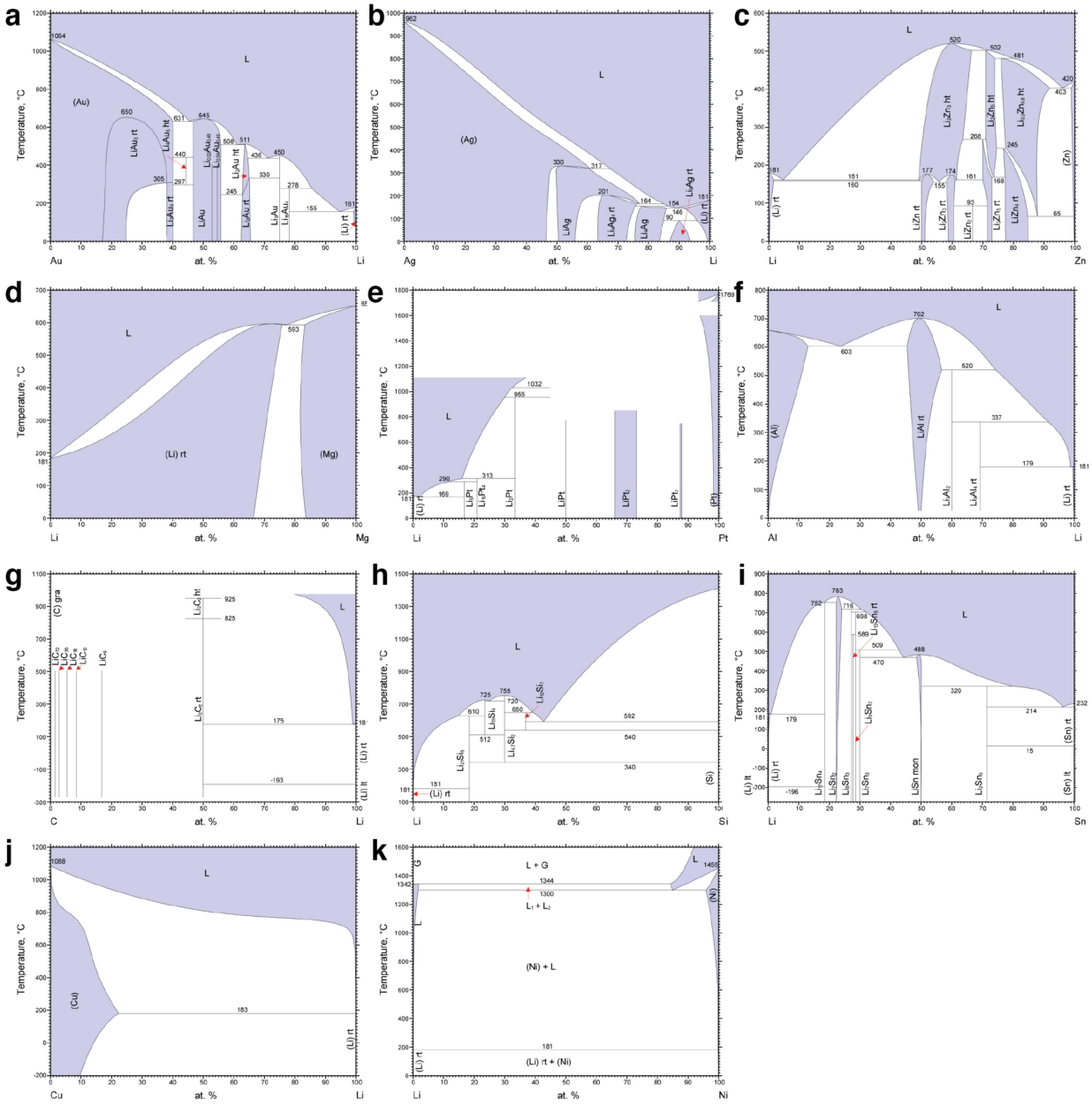

Figure S1. Li-metal binary phase diagrams. Reproduced with permissions from ref 1. Copyright 2016 Springer Nature. Data from ref 2.

Table S1. Reported critical current densities (CCDs) for garnet type ISEs. Important ISE parameter and experimental conditions, which highly expect reported CCD values, are included. The ISE properties or experimental parameters, which were basis of the respective study, are highlighted in yellow.

Composition	ρ_{rel} (%)	Micro-structure[a]	$\sigma_{ion,RT}$ (mS·cm^{-1})	$R_{P,RT}$ (Ω·cm²)	Q_{max} (mAh·cm^{-2})	ϑ (°C)	p (Mpa)	CCD (µA·cm^{-2})	ref.
$Li_{6.5}Ga_{0.15}La_3Zr_2O_{12}$	95	P (< 20 µm)	0.75	17	0.08	20	-	160	3
$Li_{6.5}Al_{0.15}La_3Zr_2O_{12}$	95	P (< 20 µm)	0.35	12	0.05	20	-	100	
$Li_{6.5}La_{2.9}Sr_{0.1}Zr_{1.4}Ta_{0.6}O_{12}$	-	P (< 5 µm)	0.39	3.5	0.30	25	-	600	4
$Li_{6.5}La_{2.9}Ca_{0.1}Zr_{1.4}Ta_{0.6}O_{12}$			0.47	5.5	0.20			400	
$Li_{6.5}La_{2.9}Ba_{0.1}Zr_{1.4}Ta_{0.6}O_{12}$			0.48	10.5	0.25			500	
$Li_{6.25}Al_{0.25}La_3Zr_2O_{12}$	96	P (5 µm)	0.46	< 5	0.14	20	3.50	300	5
	98	P (40 µm)	0.52		0.20			400	
	98	P (60 µm)	0.54		0.20			400	
	99	P (80 µm)	0.56		0.25			500	
	99	P (600 µm)	0.57		0.30			600	
$Li_{6.25}Al_{0.25}La_3Zr_2O_{12}$	90	P (20-40 µm)	0.25	130	0.025	20	0.20	50	6
	92	P (100-200 µm)	0.20	37	0.07			140	
$Li_{6-3x}Al_xLa_3Zr_2O_{12}$	-	P (5-20 µm)	0.36	500	0.78	100	-	390	7
	-	P (< 1 µm)	0.44	300	3.80	100	-	1900	
$Li_{6.5}La_3Zr_{1.5}Ta_{0.5}O_{12}$	96	P (1-3 µm)	0.66	47-69	0.08	25	1.4	150	8
		different GB	0.72		0.20			400	
		structure	0.76		0.30			600	
$Li_{6.4}Ga_{0.2}La_3Zr_2O_{12}$	100	S	1	13	0.09	20	0	280	9
				56	0.08			240	
				116	0.07			200	
				253	0.04			120	
				797	0.02			60	
				2335	0.01			40	
$Li_{6.5}La_3Zr_{1.5}Ta_{0.5}O_{12}$	96	P	0.69	400	0.1	25	1.40	200	10
				69	0.2			400	
$Li_{6.55}La_3Zr_{1.55}Ta_{0.45}O_{12}$	92-93	P (5 µm)	0.9-1	25	0.36	25	-	360	11
				100	0.11		-	110	
$Li_{6.6}La_3Zr_{1.6}Ta_{0.4}O_{12}$	> 98	P (1-2 µm)	-	18	1.00	20	0.15	500	12
				2100	0.20			100	
$Li_{6.75}Al_{0.08}La_3Zr_2O_{12}$	-	P	0.32	< 50	0.25	20	-	500	13
	-	P	0.16	< 150	0.05			100	
$Li_{6.25}Al_{0.25}La_3Zr_2O_{12}$	97	P (5-10 µm)	0.46	514	0.05	30	0.35	50	14
					0.2	70		200	
					0.8	100		800	
					3.5	130		3500	
					20	160		20000	
$Li_{6.25}Al_{0.25}La_3Zr_2O_{12}$	-	P	-	~ 10	0.2	25	3.40	900	15
						40		1400	
						60		2670	
						80		4070	
						100		6700	
$Li_{6.6}Al_{0.15}La_3Zr_{1.6}Ta_{0.4}O_{12}$	93	p (< 30 µm)	0.71	3000	0.05	25	0.10	100	16
					0.14	50		280	
					0.60	100		1200	
$Li_{6.25}Al_{0.25}La_3Zr_2O_{12}$	97	P (3 µm)	-	200	0.05	20	0.32	100	17
$Li_{6.25}Al_{0.25}La_3Zr_2O_{12}$	> 97	P	0.2	2	0.15	20	0.35	300	18
$Li_{6.25}Al_{0.25}La_3Zr_2O_{12}$	> 95	P (< 20 µm)	0.46	< 2	0.30	20	15	300	19
$Li_{6.4}La_3Zr_{1.4}Ta_{0.6}O_{12}$	94	P (10 µm)	0.2	6.95	0.36	25	5	13300[b]	20

[a] P = polycrystalline, S = single crystalline. [b] The high CCD is likely falsified by infiltration of lithium into open pores, which highly increases the effective contact area. The strong decrease of the bulk resistance in this study indicates this.

Table S2. Reported critical current densities (CCDs) for sulfide ISEs. Important ISE parameter and experimental conditions, which highly expect reported CCD values, are included. The ISE properties or experimental parameters, which were basis of the respective study, are highlighted in yellow.

Composition	ρ_{rel} (%)	Micro-structure[a]	$\sigma_{ion,RT}$ (mS·cm^{-1})	$R_{P,RT}$ (Ω·cm²)	Q_{max} (mAh·cm^{-2})	ϑ (°C)	p (Mpa)	CCD (µA·cm^{-2})	ref.
Li_3PS_4	-	P	0.26	< 100	0.1	25	-	700	21
Li_3PS_4 · LiF	-	P	0.26	< 100	0.1			>2000	
Li_2S-P_2S_5	-	A	0.5	< 70	0.40	25	-	400	22
					0.88	60	-	880	
					2.40	100	-	2400	
Li_2S-P_2S_5 (LiI)	-	A	1.8	-	1.00	25	-	1000	
					2.16	60	-	2160	
					3.90	100	-	3900	
Li_6PS_5Br	-	P	1.5	270	0.225	25	-	450	23
$Li_6PS_{4.7}O_{0.3}Br$	-	P	1.5	80	0.445	25	-	890	
Li_2S-P_2S_5	~ 80	A	0.07	-	0.50	20	0.316	500	24
	~ 80	A	0.14	-	1.00			1000	
	~ 80	A	0.12	-	0.50			500	
Li_3PS_4	~ 80	P	0.02	-	0.10			100	
Li_3PS_4 · LiI	-	A	0.79	-	0.4	25	-	400	25
					1.8	60		1800	
Li_3PS_4 · LiI	-	NC	2.27		1.0	25		1000	
					3.6	60		3600	
Li_3PS_4	-	A	0.33		0.4	25		400	
					0.6	40		600	
					1.0	60		1000	
Li_3PS_4 · LiI	-	A	0.79		1.0	60		1900	
					2.0	60		1200	
Li_2S-P_2S_5 · LiI		A	1.9	1	5	100	0.8	1700	26
Li_6PS_5Cl	-	P	0.21	-	0.35	25	-	700	27

[a] A = amorphous, P = polycrystalline, NC = nano-crystalline

Supplementary References

(1) Yan, K.; Lu, Z.; Lee, H.-W.; Xiong, F.; Hsu, P.-C.; Li, Y.; Zhao, J.; Chu, S.; Cui, Y. Selective Deposition and Stable Encapsulation of Lithium through Heterogeneous Seeded Growth. *Nat. Energy* **2016**, *1*, 16010.

(2) Okamoto, H.; Massalski, T. B. *Binary Alloy Phase Diagrams*; ASM International: Materials Park, 1990.

(3) Pesci, F. M.; Brugge, R. H.; Hekselman, A. O.; Cavallaro, A.; Chater, R. J.; Aguadero, A. Elucidating the Role of Dopants in the Critical Current Density for Dendrite Formation in Garnet Electrolytes. *J. Mater. Chem. A* **2018**, *6*, 19817–19827.

(4) Palakkathodi Kammampata, S.; Yamada, H.; Ito, T.; Paul, R.; Thangadurai, V. The Activation Entropy for Ionic Conduction and Critical Current Density for Li Charge Transfer in Novel Garnet-Type $Li_{6.5}La_{2.9}A_{0.1}Zr_{1.4}Ta_{0.6}O_{12}$ (A = Ca, Sr, Ba) Solid Electrolytes. *J. Mater. Chem. A* **2020**, *8*, 2581–2590.

(5) Sharafi, A.; Haslam, C. G.; Kerns, R. D.; Wolfenstine, J.; Sakamoto, J. Controlling and Correlating the Effect of Grain Size with the Mechanical and Electrochemical Properties of $Li_7La_3Zr_2O_{12}$ Solid-State Electrolyte. *J. Mater. Chem. A* **2017**, *5*, 21491–21504.

(6) Cheng, L.; Chen, W.; Kunz, M.; Persson, K.; Tamura, N.; Chen, G.; Doeff, M. Effect of Surface Microstructure on Electrochemical Performance of Garnet Solid Electrolytes. *ACS Appl. Mater. Interfaces* **2015**, *7*, 2073–2081.
(7) Matsuki, Y.; Noi, K.; Deguchi, M.; Sakuda, A.; Hayashi, A.; Tatsumisago, M. Lithium Dissolution/Deposition Behavior of Al-Doped $Li_7La_3Zr_2O_{12}$ Ceramics with Different Grain Sizes. *J. Electrochem. Soc.* **2019**, *166*, A5470-A5473.
(8) Basappa, R. H.; Ito, T.; Morimura, T.; Bekarevich, R.; Mitsuishi, K.; Yamada, H. Grain Boundary Modification to Suppress Lithium Penetration through Garnet-Type Solid Electrolyte. *J. Power Sources* **2017**, *363*, 145–152.
(9) Flatscher, F.; Philipp, M.; Ganschow, S.; Wilkening, M.; Rettenwander, D. The Natural Critical Current Density Limit for $Li_7La_3Zr_2O_{12}$ Garnets. *J. Mater. Chem. A* **2020**.
(10) Basappa, R. H.; Ito, T.; Yamada, H. Contact between Garnet-Type Solid Electrolyte and Lithium Metal Anode: Influence on Charge Transfer Resistance and Short Circuit Prevention. *J. Electrochem. Soc.* **2017**, *164*, A666-A671.
(11) Santhosha, A. L.; Medenbach, L.; Buchheim, J. R.; Adelhelm, P. The Indium−Lithium Electrode in Solid-State Lithium-Ion Batteries: Phase Formation, Redox Potentials, and Interface Stability. *Batteries Supercaps* **2019**, *2*, 524–529.
(12) Motoyama, M.; Tanaka, Y.; Yamamoto, T.; Tsuchimine, N.; Kobayashi, S.; Iriyama, Y. The Active Interface of Ta-Doped $Li_7La_3Zr_2O_{12}$ for Li Plating/Stripping Revealed by Acid Aqueous Etching. *ACS Appl. Energy Mater.* **2019**, *2*, 6720–6731.
(13) Wang, C.; Xie, H.; Ping, W.; Dai, J.; Feng, G.; Yao, Y.; He, S.; Weaver, J.; Wang, H.; Gaskell, K. A General, Highly Efficient, High Temperature Thermal Pulse toward High Performance Solid State Electrolyte. *Energy Storage Mater.* **2019**, *17*, 234–241.
(14) Sharafi, A.; Meyer, H. M.; Nanda, J.; Wolfenstine, J.; Sakamoto, J. Characterizing the Li–$Li_7La_3Zr_2O_{12}$ Interface Stability and Kinetics as a Function of Temperature and Current Density. *J. Power Sources* **2016**, *302*, 135–139.
(15) Wang, M.; Wolfenstine, J. B.; Sakamoto, J. Temperature Dependent Flux Balance of the Li/$Li_7La_3Zr_2O_{12}$ Interface. *Electrochim. Acta* **2019**, *296*, 842–847.
(16) Tsai, C.-L.; Roddatis, V.; Chandran, C. V.; Ma, Q.; Uhlenbruck, S.; Bram, M.; Heitjans, P.; Guillon, O. $Li_7La_3Zr_2O_{12}$ Interface Modification for Li Dendrite Prevention. *ACS Appl. Mater. Interfaces* **2016**, *8*, 10617–10626.
(17) Cheng, E. J.; Sharafi, A.; Sakamoto, J. Intergranular Li Metal Propagation through Polycrystalline $Li_{6.25}Al_{0.25}La_3Zr_2O_{12}$ Ceramic Electrolyte. *Electrochim. Acta* **2017**, *223*, 85–91.
(18) Sharafi, A.; Kazyak, E.; Davis, A. L.; Yu, S.; Thompson, T.; Siegel, D. J.; Dasgupta, N. P.; Sakamoto, J. Surface Chemistry Mechanism of Ultra-Low Interfacial Resistance in the Solid-State Electrolyte $Li_7La_3Zr_2O_{12}$. *Chem. Mater.* **2017**, *29*, 7961–7968.
(19) Krauskopf, T.; Mogwitz, B.; Rosenbach, C.; Zeier, W. G.; Janek, J. Diffusion Limitation of Lithium Metal and Li–Mg Alloy Anodes on LLZO Type Solid Electrolytes as a Function of Temperature and Pressure. *Adv. Energy Mater.* **2019**, *9*, 1902568.
(20) Zheng, H.; Wu, S.; Tian, R.; Xu, Z.; Zhu, H.; Duan, H.; Liu, H. Intrinsic Lithiophilicity of Li–Garnet Electrolytes Enabling High-Rate Lithium Cycling. *Adv. Funct. Mater.* **2019**, *30*, 1906189.
(21) Fan, X.; Ji, X.; Han, F.; Yue, J.; Chen, J.; Chen, L.; Deng, T.; Jiang, J.; Wang, C. Fluorinated Solid Electrolyte Interphase Enables Highly Reversible Solid-State Li Metal Battery. *Sci. Adv.* **2018**, *4*, eaau9245.

(22) Han, F.; Yue, J.; Zhu, X.; Wang, C. Suppressing Li Dendrite Formation in Li_2S-P_2S_5 Solid Electrolyte by LiI Incorporation. *Adv. Energy Mater.* **2018**, *8*, 1703644.
(23) Zhang, Z.; Zhang, L.; Yan, X.; Wang, H.; Liu, Y.; Yu, C.; Cao, X.; van Eijck, L.; Wen, B. All-in-one Improvement toward Li_6PS_5Br-based Solid Electrolytes Triggered by Compositional Tune. *J. Power Sources* **2019**, *410*, 162–170.
(24) Garcia-Mendez, R.; Mizuno, F.; Zhang, R.; Arthur, T. S.; Sakamoto, J. Effect of Processing Conditions of $75Li_2S$-$25P_2S_5$ Solid Electrolyte on its DC Electrochemical Behavior. *Electrochim. Acta* **2017**, *237*, 144–151.
(25) Bonnick, P.; Niitani, K.; Nose, M.; Suto, K.; Arthur, T. S.; Muldoon, J. A High Performance All Solid State Lithium Sulfur Battery with Lithium Thiophosphate Solid Electrolyte. *J. Mater. Chem. A* **2019**, *7*, 24173–24179.
(26) Suyama, M.; Kato, A.; Sakuda, A.; Hayashi, A.; Tatsumisago, M. Lithium Dissolution/Deposition Behavior with Li_3PS_4-LiI Electrolyte for All-Solid-State Batteries Operating at High Temperatures. *Electrochim. Acta* **2018**, *286*, 158–162.
(27) Zhang, Z.; Zhang, L.; Liu, Y.; Yan, X.; Xu, B.; Wang, L.-m. One-step Solution Process toward Formation of Li_6PS_5Cl Argyrodite Solid Electrolyte for All-Solid-State Lithium-ion Batteries. *J. Alloy. Compd.* **2020**, *812*, 152103.